Journal of Sound and Vibration 330 (2011) 5333–5344

Contents lists available at ScienceDirect

Journal of Sound and Vibration

journal homepage: www.elsevier.com/locate/jsvi

Surface wave transmission measurements across distributed surface-breaking cracks using air-coupled sensors

Seong-Hoon Kee, Jinying Zhu *

The University of Texas at Austin, Civil, Architectural and Environmental Engineering Department-STR, 1 University Station C1748, Austin, TX 78712-0273, USA

ARTICLE INFO

Article history:
Received 12 November 2010
Received in revised form
14 May 2011
Accepted 25 May 2011
Handling Editor: Y. Auregan
Available online 17 June 2011

ABSTRACT

Near-field scattering of surface waves by a single surface-breaking crack in solid medium has been well investigated by prior researchers. However, there have been few studies for more realistic problems involving near scattering of surface waves by distributed surface-breaking cracks. One possible reason is complexity caused by the interaction of surface waves between multiple cracks. In this study, interaction of surface waves between two surface-breaking cracks with various crack spacing was investigated. The experimental study was performed on Plexiglas specimens with non-contact sensors (air-coupled sensors, and a laser vibrometer), and compared with numerical simulation results. The effects of crack depth h, spacing a, and the number of cracks N on surface wave transmission were studied. Analyses show that for the very small crack spacing ($a/h < 0.2$), the distributed cracks can be regarded as a single surface-breaking crack. However, for a/h ranging between approximately 1 and 6, transmission coefficient of surface waves is significantly affected by interaction between cracks. The transmission coefficients have the lowest value when a/h is between 2 and 3. When a/h is large ($a/h > 6$), transmission coefficients obtained from experiments, and numerical simulations agree with the theoretical results based on non-interaction crack assumption.

1. Introduction

Surface waves are mechanical waves propagating along the surface of solid materials with both longitudinal and transverse motion [1]. Most energy of surface waves is confined near the free surface of a solid body with frequency-dependent penetration depth. The low frequency components have deep penetration. A single surface-breaking crack normal to the free surface causes scattering of surface waves at the crack, and attenuates incident surface waves by diffraction, reflection, transmission, and mode conversion [2]. Scattering of surface waves caused by a surface-breaking crack (or slot) has been extensively studied by experimental studies and numerical simulations since late 1970s. Achenbach and his colleagues [3–5] obtained analytic solutions for scattering field of surface waves interacting with a single surface-breaking crack. Based on the scattering theory, reflection and transmission coefficients of surface waves in the far field of a crack were presented in terms of the normalized crack depth (h/λ, crack depth normalized by wave length of surface waves). Hirao et al. [2] investigated scattering of surface waves by a surface-breaking crack through numerical simulations (finite element method) and experimental measurements in a wide frequency range ($h/\lambda = 0$–3.0). Yew et al. [6] measured transmission coefficients of surface waves across a surface-breaking crack through experimental studies. They pointed out difficulties to interpret the signal data measured in the near field of a crack caused by crack tip scattering. Masserey and Mazza [7] observed oscillations in reflection and transmission coefficients of surface

* Corresponding author. Tel.: +1 512 232 5502.
E-mail addresses: seonghoonkee@utexas.edu (S.-H. Kee), jyzhu@mail.utexas.edu (J. Zhu).

0022-460X/$ - see front matter © 2011 Elsevier Ltd. All rights reserved.
doi:10.1016/j.jsv.2011.05.034

waves across a surface-breaking crack measured in near field of the crack. Jian et al. [8] discussed a mechanism of signal enhancements in near field of a crack, and oscillation in surface wave reflection and transmission coefficients by means of multiple reflected and transmitted waves at the crack. The authors of this paper proposed an approximate near-field size based on numerical simulations (FEM) and experiments [9].

Although the scattering of surface waves by a single surface-breaking crack have been well studied, there has been very few experimental works for more realistic problems involving distributed surface-breaking cracks in solid medium. The dispersion and scattering of surface waves caused by non-interacting distributed surface-breaking cracks has been studied by Zhang and Achenbach [10]. In that study, crack spacing was assumed large enough so that there was no interaction between cracks. They studied phase velocity and attenuation coefficients of surface waves across uniformly distributed surface-breaking crack based on the non-interaction assumption. Recently, Pecorari [11,12] suggested an effective field approach to model the dispersion and attenuation of surface waves across distributed cracks. Until now, an exhaustive theoretical model describing the interaction of surface waves between distributed surface cracks has not yet been developed. This is mainly due to the complexity of surface wave interaction between individual surface-breaking cracks.

In addition to non-destructive evaluation of solids with cracks, another application of the scattering theory is to design effective vibration insulation of ground-transmitted surface waves. The application of a trench and a sheet-wall barrier to isolate a sensitive instrument in laboratory was reported by McNeill et al. [13]. Woods [14] performed a series of field experiments to investigate effectiveness of trench and sheet-wall barriers for vibration isolation, and presented guidelines for the dimensions of an open trench to achieve a ground amplitude reduction of 75% or more. Comprehensive literature reviews of this topic have been reported by previous researchers [15–17]. Generally, a trench is regarded as effective for vibration insulation; however, sometimes, practical use of a trench is limited to small or medium trench depth because of soil instability, and high underground water level. In this sense, better understanding of surface-wave scattering in the near field of various distributed cracks (or slots) will help achieve effective vibration insulation.

In surface wave transmission measurement, inconsistent sensor coupling condition is a challenge to obtain accurate and consistent signals over surface-breaking cracks in a solid. Using non-contact sensors (air-couple sensors, and/or a laser vibrometer) provides a solution to the sensor contact problem in experimental measurements. Air-coupled sensors have been successfully used to measure leaky Rayleigh waves or Lamb waves by Zhu and Popovics [18]. The authors [9] also demonstrated that using air-coupled sensors significantly improved accuracy and test speed in surface wave transmission measurements on concrete. Compared to contact sensors, the air-coupled sensors allow rapid and more consistent measurement by eliminating sensor contact.

In this study, near-field scattering of surface waves interacting with distributed surface-breaking cracks is investigated through experimental measurements using non-contact sensors (air-coupled sensors and a laser vibrometer), and numerical simulations (FEM). An experimental program and test setup are shown in Section 2. Section 3 contains a brief description of FE models for numerical simulations developed in this study. Verification of the FE models is shown in Section 4.1. Based on the results from experimental studies and numerical simulations, interaction of surface waves between individual surface-breaking cracks are investigated in Section 4.2. In addition, effects of crack spacing a, and the number of cracks N on the transmission coefficients of surface waves are discussed for a wide range of normalized crack depth h/λ in Section 4.3.

From the practical standpoint, surface wave transmission across surface-breaking cracks is also affected by geometry and partially closed interface of the cracks. In this paper, however, notch-typed cracks were used in numerical simulations and experimental studies for simplicity, which provides a good starting point to investigate more complex problems. For real cracks with partial contact interfaces, the authors will present experimental studies in a separate paper.

2. Laboratory experiment

2.1. Preparation of test specimens

Two series of Plexiglas (Poly methyl methacrylate, PMMA) specimens with sizes of $600 \times 230 \times 6.35\ mm^3$ (series A), and $1200 \times 300 \times 25.4\ mm^3$ (series B) were prepared for measuring near-scattering field of surface waves and surface wave transmission across various distributed cracks in laboratory. In this study, the Plexiglas specimen was held in upright position as shown in Fig. 1. The Plexiglas specimens of series A include five specimens, in which three have two surface-breaking cracks, one has a single crack and one does not contain any crack. All cracks have the same depth of 8 mm, and crack spacings of 0, 8, 24, and 48 mm. Similarly, the specimens of series B include 10 specimens with various numbers of cracks of 1, 2, 3, and 4 and one specimen without crack. The cracks have the same depth of 15 mm, and various spacings of 0, 15, 45, and 90 mm. Consequently, this test program covers four spacing-to-depth ratios ($a/h=0$, 1, 3, and 6) of distributed surface-breaking cracks in Plexiglas. The characteristics of Plexiglas specimens are summarized in Table 1. The specimens are named based on test variables. For example, A2-24-8 indicates the Plexiglas specimen series A having 2 surface-breaking cracks with a spacing 24 mm, and a depth 8 mm. A hand saw was used to generate surface-breaking cracks perpendicular to the free surface of specimens. The width of all cracks is approximately 0.5 mm. The width-to-depth ratios of cracks used in this study are around 1/16 and 1/30 for series A and B, respectively. Note that these values are small enough to ignore effects of the crack width on transmission coefficients of surface waves according to Masserey and Mazza [7]. Therefore, the results from the experimental study can be directly compared with analytic results. The

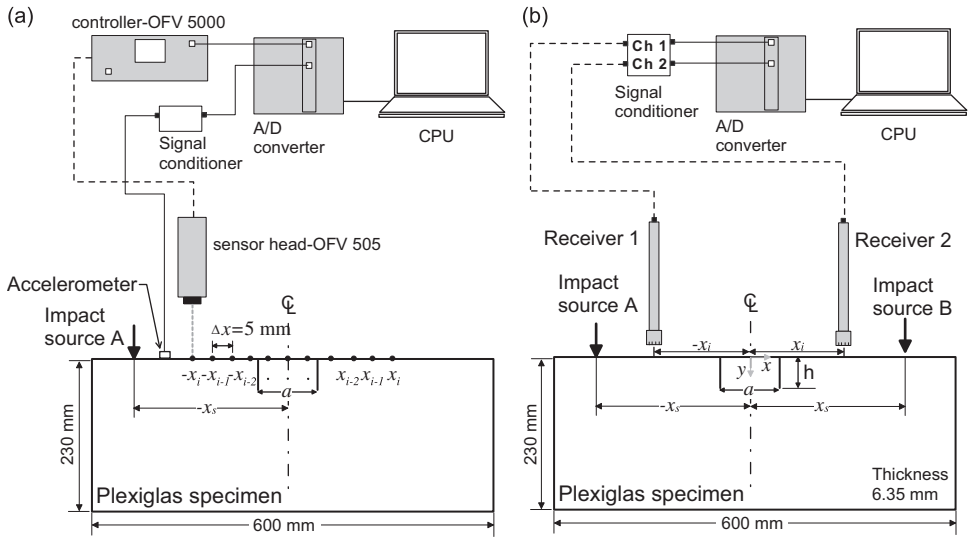

Fig. 1. Experimental setup and data acquisition system for (a) a laser vibrometer and (b) air-coupled sensors on the Plexiglas specimen series A with an impact source having duration T around 40 μs ($\lambda \sim 50$ mm).

Table 1
Properties of Plexiglas specimens for experiments.

Plexiglas specimens	Specimen size	Crack spacing a (mm)	Crack depth h (mm)	# of cracks N	a/h	Center frequency f_c (kHz)
Series A						
A0-0-0 (no crack)	$600 \times 230 \times 6.35$ (mm^3)	0	0	0	0	25
A1-0-8 (single crack)		0	8	1	0	
A2-8-8		8		2	1	
A2-24-8		24		2	3	
A2-48-8		48		2	6	
Series B						
B0-0-0 (no crack)	$1200 \times 300 \times 2.54$ (mm^3)	0	0	0	0	15
B1-0-15 (single crack)		0	15	1	0	
B2-15-15		15		2	1	
B2-45-15		45		2	3	
B2-90-15		90		2	6	
B3-15-15		15		3	1	
B3-45-15		45		3	3	
B3-90-15		90		3	6	
B4-15-15		15		4	1	
B4-45-15		45		4	3	
B4-90-15		90		4	6	

Note: A2-24-8 means a Plexiglas specimen series A containing 2 surface-breaking cracks with a spacing of 24 mm and a depth of 8 mm.

phase velocity of surface waves obtained from the spectral analysis of surface wave (SASW) test converges to 1245 m/s when frequency is greater than 15 kHz. This velocity is compatible with the value of 1244 m/s calculated based on generalized plane stress approximation [19] for Young's modulus E of 5800 MPa, Poisson's ratio ν of 0.33, and mass density ρ of 1190 kg/m^3. This also demonstrates that the thickness of specimens and frequency range ($H/2\lambda_r > 1$) implemented in this study are appropriate for surface wave propagation.

2.2. Test setup and data acquisition

2.2.1. Near-scattering field measurement using a laser vibrometer

A schematic view of the test setup for the Plexiglas specimen series A is shown in Fig. 1(a). A laser vibrometer by Polytec (sensor head-OFV 505 and controller-OFV 5000) was used to measure vertical velocity responses in near-scattering field of distributed-surface breaking cracks in Plexiglas specimens. The specimens were moved to scan the surface of specimens from $x_i = -200$ to 200 mm at an interval of 5 mm, where x_i is the distance of the sensor from the midpoint between two cracks (see Fig. 1(a)). An accelerometer was installed near the impact point to calibrate the impact force.

2.2.2. Surface wave transmission measurement using air-couple sensors

To measure surface wave transmission, two air-coupled sensors (PCB model No. 377B01) were located at $-x_i$ and x_i from the centerline of the specimens (see Fig. 1(b)). In this study, x_i varies from 10 to 150 mm at an interval of 10 mm to investigate the effects of sensor locations on transmission coefficients. The impact source was applied at $x_S = \pm 200$ mm. Test setup for the Plexiglas specimen series B is the same as that for the specimens series A, except that the impact source was located at $x_S = \pm 300$ mm. The air-coupled sensing technique has been described in more detail in another publication [9].

To reduce experimental variability in the surface wave measurement, signal data were acquired through the self-calibrating procedure [20–22]. The surface wave transmission ratios were measured from opposite directions, and averaged as follows:

$$\mathrm{Tr} = \sqrt{\frac{\mathbf{S}(-x_S, x_i)\mathbf{S}(x_S, -x_i)}{\mathbf{S}(-x_S, -x_i)\mathbf{S}(x_S, x_i)}}, \tag{1}$$

where $\mathbf{S}(\pm x_S, \pm x_i)$ are the Fourier transform of the time signal data $\mathbf{V}(\pm x_S, \pm x_i)$ generated by impact sources at $\pm x_S$ and recorded by the sensors located at $\pm x_i$.

In addition, five repeated signal data sets were collected at the same test location to improve signal consistency. These five transmission functions were then arithmetically averaged in frequency domain. To evaluate the consistency of obtained signals generated by the left impact at $-x_S$, the signal coherence function defined as follows:

$$\mathbf{SC}_{12}(f) = \frac{\left|\sum_{j=1}^{5} \mathbf{G}_{12,j}(f)\right|^2}{\sum_{j=1}^{5} \mathbf{G}_{11,j}(f) \times \sum_{j=1}^{5} \mathbf{G}_{22,j}(f)}, \tag{2}$$

where $\mathbf{G}_{12,j}(f)$, $\mathbf{G}_{11,j}(f)$ and $\mathbf{G}_{22,j}(f)$ are the cross spectrum and auto spectrum functions between $\mathbf{V}(-x_S, x_i)$ and $\mathbf{V}(-x_S, -x_i)$ obtained from the signal data set with index j. Similarly, $\mathbf{SC}_{21}(f)$ can also be calculated from signals $\mathbf{V}(x_S, x_i)$ and $\mathbf{V}(x_S, -x_i)$ generated by the right impact at $+x_S$. The averaged $\mathbf{SC}(f)$ is defined as

$$\mathrm{SC}(f) = \sqrt{\mathbf{SC}_{12}(f) \times \mathbf{SC}_{21}(f)}. \tag{3}$$

$\mathbf{SC}(f)$ ranges from 0 to 1.0. A value close to 1.0 indicates good signal quality and repeatability. The signal coherence function was used to determine the acceptable frequency range of a transmission ratio curve.

The measured surface wave transmission coefficients Tr were normalized by Tr_0, which is the transmission coefficient obtained from a crack free specimen. All analyses were performed in the frequency domain. A *Hanning* window was applied to the time domain signals to extract the surface wave components.

Transient forces were generated by dropping a steel ball guided by a plastic tube. The ball diameters are 3 and 6.35 mm for the Plexiglas specimen series A and B, respectively. They generate incident surface waves having center frequencies around 25, and 15 kHz, and provide good signal consistency up to 50 and 30 kHz. The acquired signals were digitized at a sampling frequency of 1 MHz using an NI-USB 5133 oscilloscope.

3. Numerical simulation

3.1. Model description

Finite element method (FEM) was used to simulate the transient behavior and near-field scattering of surface waves caused by distributed surface-breaking cracks in Plexiglas specimens. The main purpose of numerical simulation in this study is to investigate wide range of variables, which could not be completely covered by the experimental program. The main variables in the numerical simulation are *crack depth h, crack spacing a, and the number of crack N*.

To save computational cost, 2D FE models with distributed surface-breaking cracks were developed using rectangular plane stress elements (CPS4) in a finite element package (ABAQUS *v 6.7.1*) as shown in Fig. 2. Plane stress elements (CPS4) were verified to effectively simulate the transient behavior of surface waves across a surface-breaking crack by the authors. In this study, the FE model was extended to investigate near-field scattering of surface waves interacting with distributed surface-breaking cracks. The mesh size was designed 2 mm so that at least 25 elements can participate to

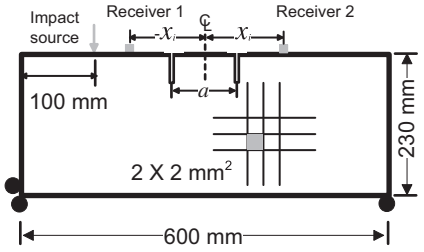

Fig. 2. A finite element model containing two surface breaking cracks with the spacing a, and the same depth h.

express the minimum wavelength λ_{min} [23]. In addition, the time increment Δt for integration was determined to be 1 μs to maintain accuracy [24]. In addition, the default numerical damping ($\alpha = -0.05$) given by ABAQUS was used to ensure solution convergence. To reasonably simulate energy dissipation per cycle, material damping was also defined based on linear Rayleigh damping model. The damping ratio is defined as $D = \eta_1/2\omega + \eta_2\omega/2$, where η_1 and η_2 are constants for mass and stiffness, and ω is angular frequency of waves [25]. The constants η_1 and η_2 were set to 2700 and 5×10^{-8} for Plexiglas specimens so that D was approximately 0.015 in the frequency range of 10–50 kHz. A transient impact source was applied on the free surface at the location of $x = -200$ mm. The force function of the impact point source is

$$f(t) = \sin^2(\pi t/T), \quad 0 \le t \le T, = 0, \quad t > T. \tag{4}$$

where T is the duration of transient force. The quadratic force function in Eq. (4) was verified effective to simulate the transient contact forces by previous researchers [26]. Material properties of Plexiglas were assumed homogeneous and linear-elastic. This is valid and reasonable within the frequency range in this study (i.e., center frequency $f_c \sim 15$, and 25 kHz), and reduces complexity of numerical simulation. Material properties of Plexiglas were selected as Young's modulus E of 5800 MPa, Poisson's ratio ν of 0.33, and mass density ρ of 1190 kg/m^3. The corresponding velocities of P-, S-, and surface waves were 2338, 1353, and 1244 m/s, respectively.

3.2. Determination of surface wave transmission

Transmission coefficients of surface waves across distributed cracks were investigated in the frequency domain. Parameters affecting the surface wave transmission include frequency f, crack depth h, crack spacing a, and the number of crack N. The surface wave transmission coefficient **Tr** is defined as the amplitude frequency response ratio between the cracked model and the crack free model as follows:

$$\mathbf{Tr}_n(f,h,a,N) = \frac{\mathbf{S}_2(h)}{\mathbf{S}_1(h)} \Big/ \frac{\mathbf{S}_2(0)}{\mathbf{S}_1(0)}, \tag{5}$$

where $\mathbf{S}_1$ and $\mathbf{S}_2$ are the Fourier transforms of the vertical velocity responses measured by sensors 1 and 2 (see Fig. 2). Similar to the procedure described in Section 2.2, a window function (*Hanning* window) with a length of two periods was applied at the surface wave components before the Fourier transform [21,22].

4. Results and discussion

4.1. Verification of FE model

The validity of the finite element model was investigated by comparison with experimental results. Each vertical velocity response $V_y(x/\lambda,t)$ calculated from the finite element model and measured by a laser vibrometer on the free surface of the Plexiglas was normalized by its negative peak value $\min(V_y(x/\lambda,t))$, where x is the distance from the midpoint between two cracks, and t is time. Fig. 3 compares the normalized vertical velocity response of signal data obtained from the FE model and the Plexiglas specimen A1-0-8 (refer to Table 1). The six signal data sets were measured at six locations ($x = \pm 20$, ± 60, and ± 100 mm) on the free surface of the specimen. The first arrivals are P waves, and then, mode converted S waves (PS: P waves

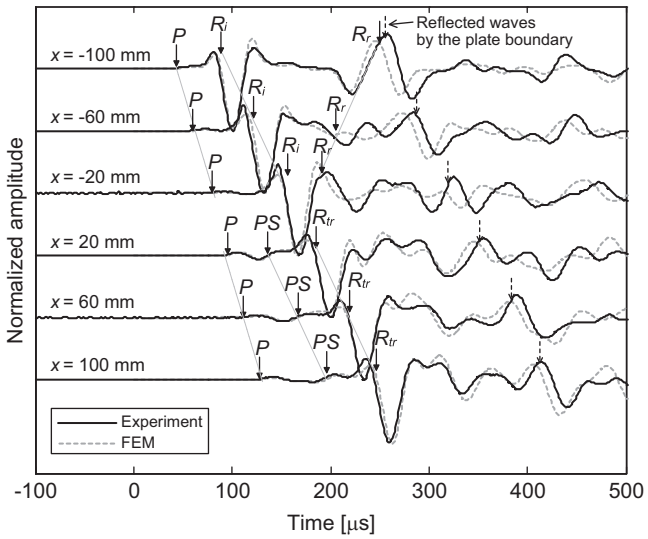

Fig. 3. Comparison of responses in near-scattering fields measured using a laser vibrometer from the Plexiglas specimen of P0-8 and from FE model.

to S waves) follow. In the backward scattering field, the incident surface waves (R_i), the reflected waves (R_r) from a crack and from the left boundary of the specimen are clearly seen in the time domain. In the forward scattering field, transmitted surface waves (R_{tr}) across a crack, and reflected surface waves from the plate boundary can be seen in the time domain. The normalized velocity responses from FE model match well with signals from experimental measurements. In particular, main pulses of surface waves (R_i, and R_{tr}) from the FE models show very good agreement with the corresponding measurements from the Plexiglas specimen A1-0-8. This demonstrates the validity of FE models used in this study for investigating the scattering problems of surface waves interacting with surface-breaking cracks (or slots).

4.2. Interaction of surface waves between individual cracks

Near-field scattering of surface waves interacting with two cracks with the same crack depth h was investigated. The vertical velocity responses $V_y(x,t)$ were obtained from numerical simulations (FEM) and experimental measurements using a laser vibrometer described in Sections 2 and 3.

Figs. 4 and 5 show the B-scan images representing the near-field scattering of surface waves interacting with two surface-breaking cracks obtained from the FE analyses and experiments, respectively. It can be seen that the experimental measurements agree with the numerical simulations well. In all models and specimens, the cracks have the depth of 8 mm, and spacings of 0, 8, 24, and 48 mm. Consequently, four crack-spacing-to-depth ratios a/h of 0, 1, 3, and 6 are covered in Figs. 4 and 5. Interaction of surface waves between two cracks substantially affects the backward and forward scattering field of surface waves. Figs. 4 (a) and 5(a) illustrate the scattering field by a single surface-breaking crack. The reflected surface waves (R_r) by a surface-breaking crack, the transmitted waves (R_{tr}) across the crack, and reflected surface waves by the plate boundary (R_{2i}) are clearly seen. The dark color in the B-scan images indicates the negative amplitude of waves, and the light color for positive amplitude. Figs. 4(b) and 5(b) show surface waves scattered by two cracks with small spacing ($a/h=1$). The surface waves trapped between two cracks generate multiple reflections and transmissions into the backward and forward scattering fields. Increasing crack spacing to 24 mm ($a/h=3$) results in complex near-scattering field before and after cracks, as shown in Figs. 4(c) and 5(c). In the backward scattering field, the reflected waves

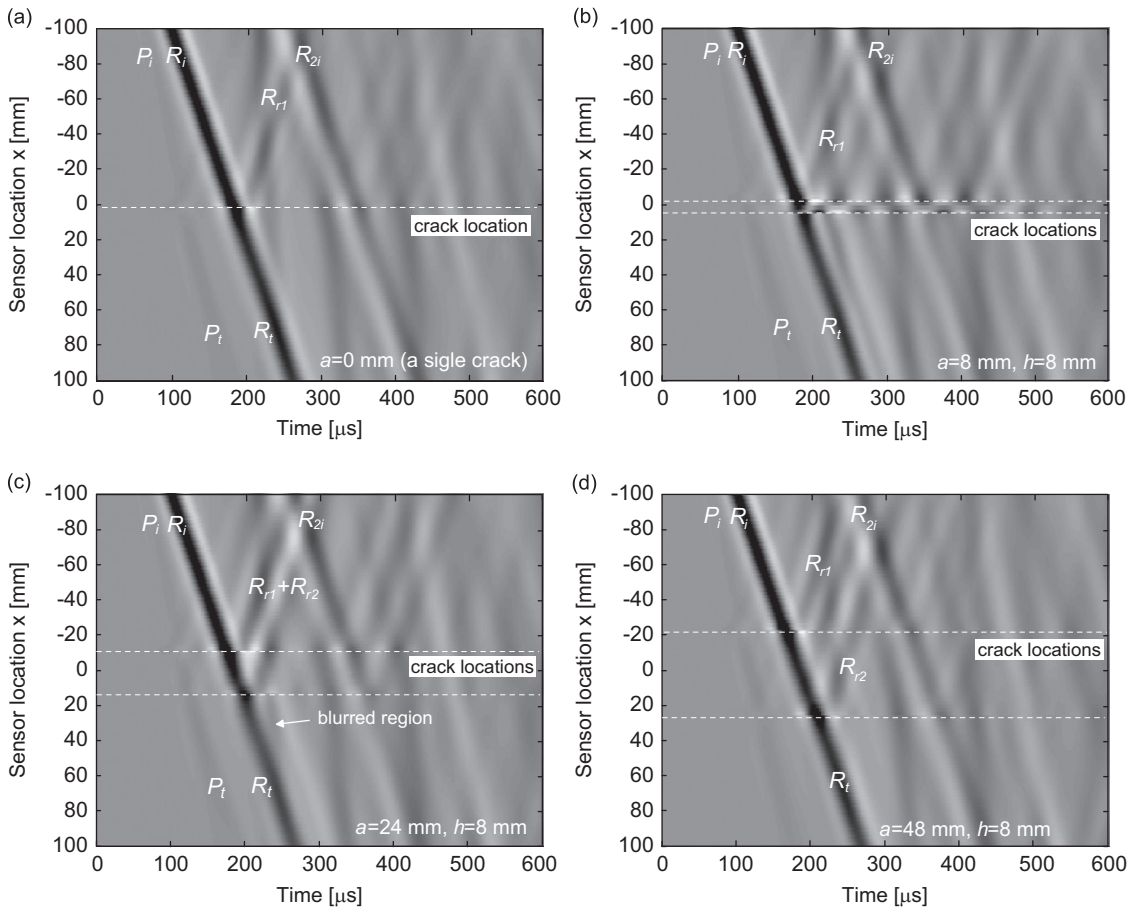

Fig. 4. Surface wave response $V_y(x,t)$ in near-scattering fields caused by two surface-breaking cracks obtained from FE models with crack depth $h=8$ mm: (a) $a/h=0$ (single crack); (b) $a/h=1$; (c) $a/h=3$ and (d) $a/h=6$.

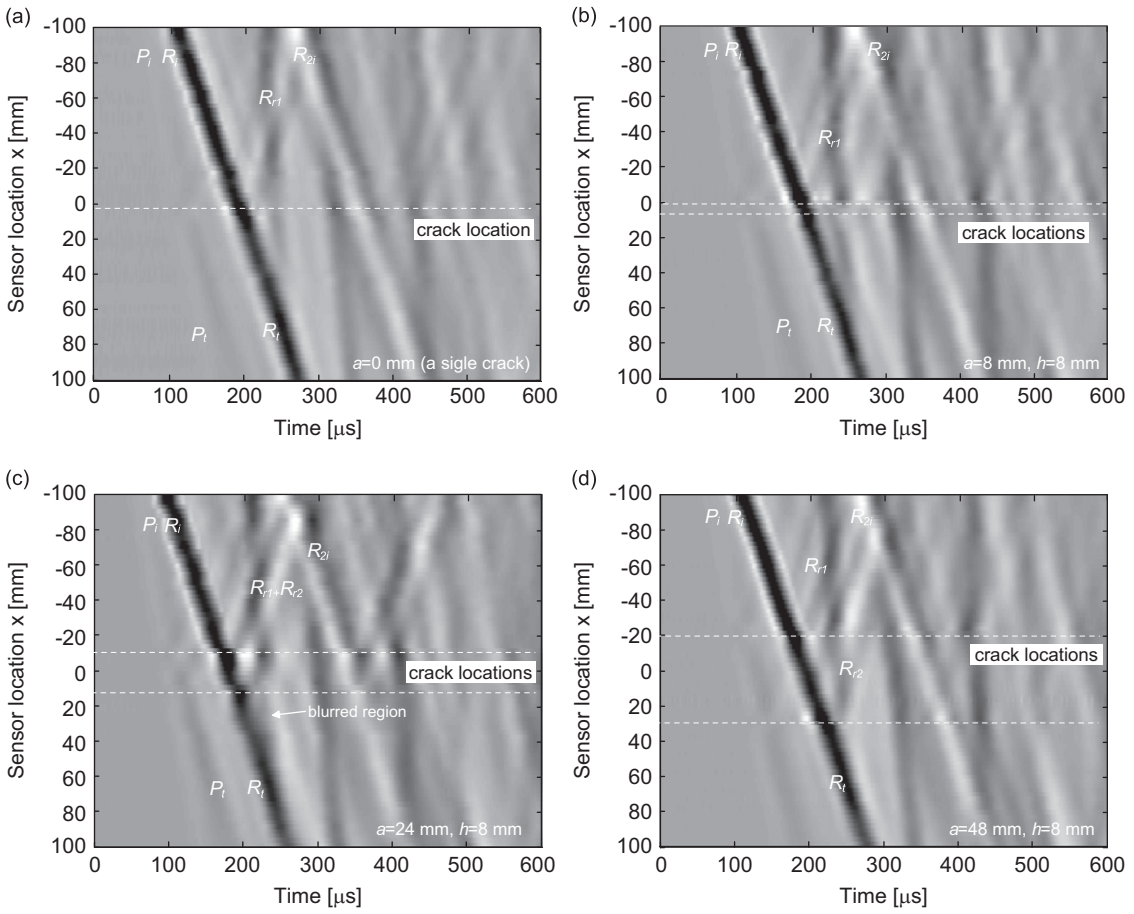

Fig. 5. Surface wave response $V_y(x,t)$ in near-scattering fields caused by two surface-breaking cracks (h=8 mm) measured using a laser vibrometer from Plexiglas specimens: (a) a/h=0 (single crack); (b) a/h=1; (c) a/h=3 and (d) a/h=6.

from the first (R_{r1}) and the next crack (R_{r2}) interfere with each other. In the forward scattering field, the transmitted surface waves are blurred and have lower amplitude. These will further affect determination of transmission coefficients of surface waves across the cracks. Figs. 4(d) and 5(d) show that further increasing the crack spacing to 48 mm (a/h=6) results in two separated waves, each of which is reflected by the first (R_{r1}) and the second cracks (R_{r2}), and there is no strong interference between these waves.

Fig. 6 shows signal amplification coefficients versus the normalized distance x/λ for the same crack depth h of 8 mm and crack spacings a of 0, 8, 16, 24, 48, 72 and 96 mm. The signal amplification coefficient (APC) is the negative peak amplitude ratio between the vertical velocity responses $\mathbf{V}_{yh}(x/\lambda,t)$ on a cracked model and that on a crack free model ($\mathbf{V}_{y0}$) as follows:

$$\mathrm{APC}(x/\lambda) = \frac{\min|\mathbf{V}_{yh}(x/\lambda,t)|}{\min|\mathbf{V}_{y0}(x/\lambda,t)|}, \tag{6}$$

where x/λ is defined as the normalized distance, x is the distance from the midpoint between cracks and λ is the wavelength of incident surface waves corresponding to the center frequency. For example, for T=40 μs, λ is approximately 50 mm in Plexiglas.

The APC curves are strongly affected by the crack spacing a even though the crack depth are the same. In addition, effects of the crack spacing on near-scattering fields of surface waves also depend on near-field size a_n. The near-field sizes a_n has been studied by the authors [9]. It was found that a_n depends on crack depth h, and wavelength λ of incident surface waves. In this study, for h=8 mm and λ=50 mm, a_n is approximately 20 mm. When a=8 mm, which is smaller than half of a_n, the APC curve is similar to that measured from a single crack model (a=0 mm). The APC curve shows oscillatory behavior in the near-field region, and then converges into a constant value for large x/λ. This value represents the surface wave transmission coefficient measured in the far field, where the measurement is not affected by sensor locations. When the crack spacing a increases but is less than $2a_n$, the forward scattering field from the first crack tip interferes with the backward scattering field from the second crack tip. Consequently, complex near-field scattering forms in the region between two cracks, as shown in Figs. 4 and 5. This interaction affects transmission measurement of surface waves across distributed surface-breaking cracks. When the crack spacing a further increases to 48, 72, and 96 mm ($a/a_n \sim$2.5, 3.5, and 5),

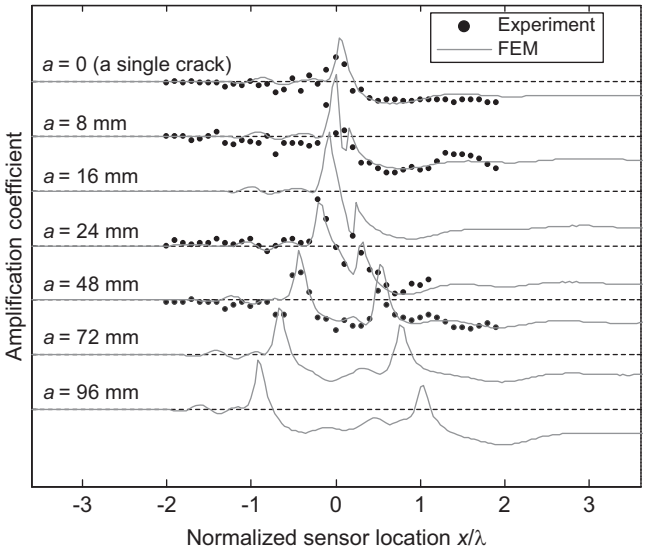

Fig. 6. Amplification coefficients versus normalized sensor location (x/λ) obtained from FE models and experiments: $\lambda=50$ mm and $h/\lambda=0.16$.

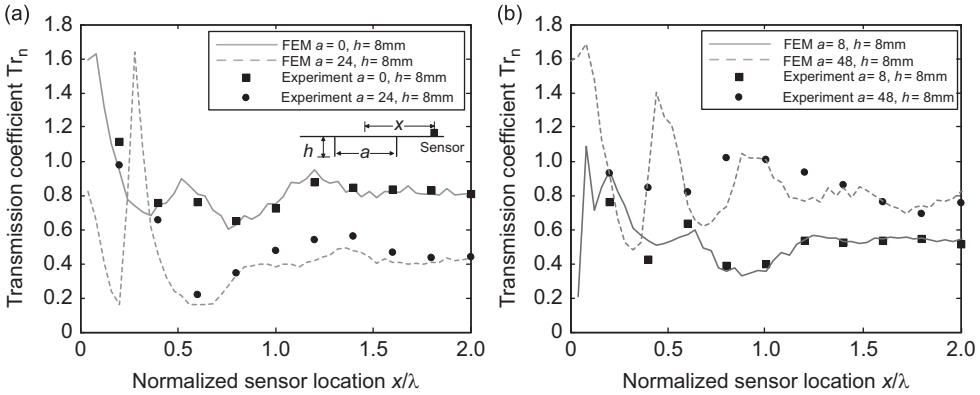

Fig. 7. Normalized transmission coefficient versus normalized sensor location (x/λ) obtained from FE models and experiments for (a) $a=0$ and 24 mm and (b) $a=8$ and 48 mm: $\lambda=50$ mm and $h/\lambda=0.16$.

interaction of surface waves between cracks considerably decreases so that the cracks can be regarded as two separated cracks. In this case, the previous surface wave transmission theories for a single crack may still be applied to each single crack. For example, if the surface wave transmission ratio after the first crack is Tr, then the transmission after the second crack will converge to Tr^2 in far field.

4.3. *Transmission coefficients Tr_n*

In this section, transmission coefficients of surface waves across distributed surface-breaking cracks were calculated in the frequency domain as described in previous Sections 2.2 and 3.2.

4.3.1. *Effects of sensor locations on Tr_n*

To obtain better understanding of near-field scattering by distributed cracks, effects of sensor locations on Tr_n were investigated through FE analyses and experimental measurements by air-coupled sensors. Fig. 7(a), and (b) present the relationship between Tr_n and the normalized sensor location x/λ. Tr_n measured from the Plexiglas specimens series A (A1-0-8, A2-8-8, A2-24-8 and A2-48-8) are presented with solid circles, and the results obtained from corresponding FE models with solid lines. Note that to avoid overlapping the plots, the results from A1-0-8 and A2-24-8, and those from A2-8-8 and A2-48-8 are plotted in Fig. 7(a) and (b), respectively. The experimental measurements show good agreement with FE models. Consistent with observations by previous researchers [7,8], the near-field scattering by a crack ($x/\lambda<0.5$) results in strong enhancement and oscillation in transmission coefficients Tr_n; while Tr_n tends to converge to a constant value when

sensors become far from the crack opening (i.e., $x/\lambda > 1.0$). The approximate near-field size for a single crack ($x/\lambda \sim 1.5$) is effective on distributed cracks. In this study, sensor locations are chosen as $x/\lambda \sim 1.5$ to ensure far-field measurements.

4.3.2. Effects of crack spacing a/h

Among the parameters which affect surface wave transmissions, preliminary analyses by the authors [27] indicated that the normalized crack spacing a/h has the largest influence on $\mathrm{Tr}_n(f_c)$ for a given number of cracks N. Fig. 8 shows the variation of $\mathrm{Tr}_n(f_c)$ with crack spacing a/h based on FE analyses and experimental measurements, where $\mathrm{Tr}_n(f_c)$ is the normalized transmission coefficient at the center frequency, as shown in Table 1. Solid squares in Fig. 8(a) are results from the specimens A1-0-8, A2-8-8, A2-24-8, and A2-48-8, and solid circles in Fig. 8(b) are of the specimens B1-0-15, B2-15-15, B2-45-15, and B2-90-15. For comparison purposes, $\mathrm{Tr}_n(f_c)$ from corresponding FE analyses are presented as dashed-line with open squares and open circles at Fig. 8(a) and (b). The experimental results show very good agreement with those from FE analyses. For the same crack depth h, $\mathrm{Tr}_n(f_c)$ has the minimum value around $a/h=2$–3, and tends to converge to a constant value Tr^2 when a/h is greater than 6. This is consistent with the results from the previous study based on non-interaction approximation.

Fig. 9 shows Tr_n–h/λ curves for different crack spacings ($a/h=0$, 0.2, 3, and 10). The transmission curves for different a/h were obtained by combining the transmission coefficients from five FE models with different h (5, 10, 15, 20, and 25 mm) in frequency range from 10 to 30 kHz. Consequently, for the same a/h, there are overlap h/λ regions. For comparison purposes, analytic solution of $\mathrm{Tr}_n(f_c)$ for a single surface-breaking crack given by Angel and Achenbach [5] were presented as a solid line. $\mathrm{Tr}_n(f_c)$ based on the non-interaction assumption (i.e., $\mathrm{Tr}_n(f_c, h, N=2)=[\mathrm{Tr}_n(f_c, h, N=1)]^2$) is also shown as a dash line in the same figure. For a single crack ($a/h=0$), the transmission from FEM analyses show good agreement with the analytic solution. When the crack spacing is very small (e.g., $a/h \sim 0.2$), $\mathrm{Tr}_n(f_c, h, N=2)$ is close to the single crack transmission curve.

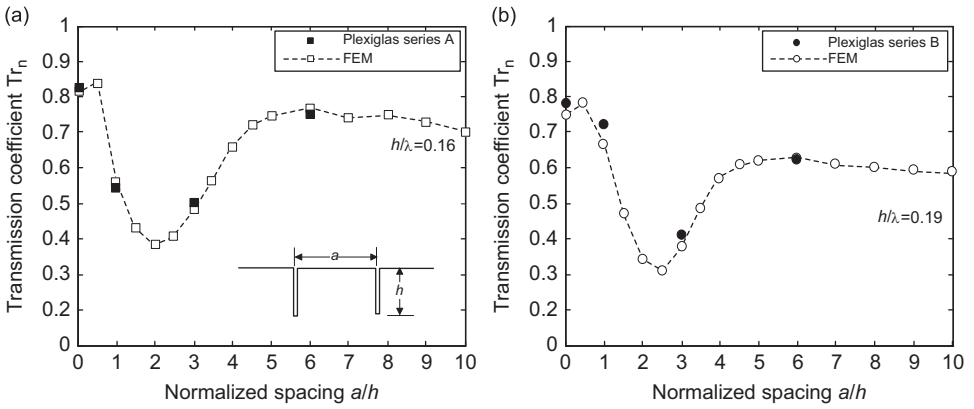

Fig. 8. Normalized transmission coefficient versus normalized sensor spacing obtained from experimental studies and FE models for (a) $h/\lambda \sim 0.16$ and (b) $h/\lambda \sim 0.19$.

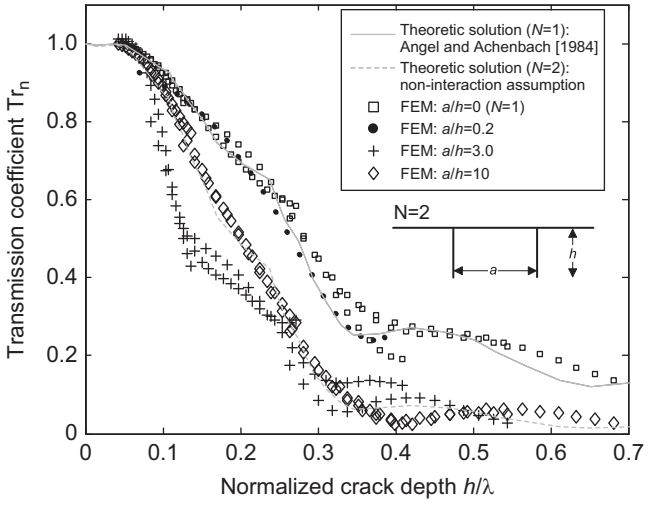

Fig. 9. Effects of crack spacing a/h on surface wave transmission coefficient.

For very large crack spacing ($a/h=10$), the FEM results converge to the dash line based on the non-interaction theory. For $a/h=3$, the interaction effect appears most significant when h/λ is approximately between 0.1 and 0.25.

4.3.3. Effects of the number of distributed cracks N on Tr_n

Fig. 10 shows $Tr_n(N)$ versus N curves obtained from FE analyses and experimental measurements from the Plexiglas specimens series B ($a/h=1$, 3, and 6 with $h=15$ mm, $f_c=15$ kHz; $h/\lambda\sim0.18$), where $Tr_n(N)$ is the transmission across N cracks. $Tr_n(N)$ is further normalized by the single crack transmission $Tr_n(1)$. Results from Plexiglas specimens corresponding to a/h of 1, 3, and 6 are presented as solid circles, solid squares and solid triangles, respectively. The surface wave transmission curve based on non-interaction theory is also presented as a solid line in Fig. 10. Consistent with the observations from the two-crack analysis, transmission coefficients of surface waves across three, and four surface-breaking cracks also have the lowest values when $a/h=3$. In addition, the Tr_n–N curve converges to the non-interaction solid line Tr^N when $a/h=6$.

4.3.4. Two surface-breaking cracks with different h

Fig. 11 shows the transmission coefficients $Tr_n(f_c)$ versus crack depth ratio h_1/h_2 between two cracks, where h_1 and h_2 are the depth of two surface-breaking cracks (see the illustration in Fig. 11). The results in Fig. 11 were obtained using the

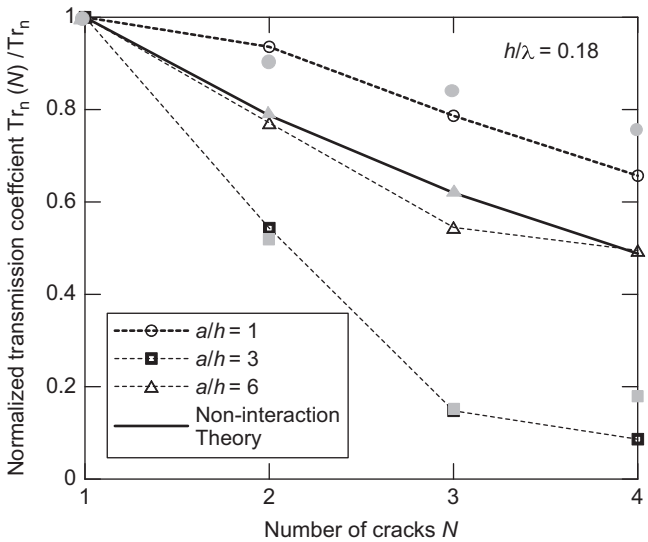

Fig. 10. Effects of crack spacing a/h on surface wave transmission coefficient for multiple cracks. The dash lines with circles, squares, and triangles are results from numerical simulation (FEM) of $a/h=1$, 3, and 6, respectively; solid circles, solid squares, and solid triangles are obtained from experiments using Plexiglas specimens with $a/h=1$, 3, and 6, respectively; and the solid line is corresponding to the theory based on non-interaction assumption.

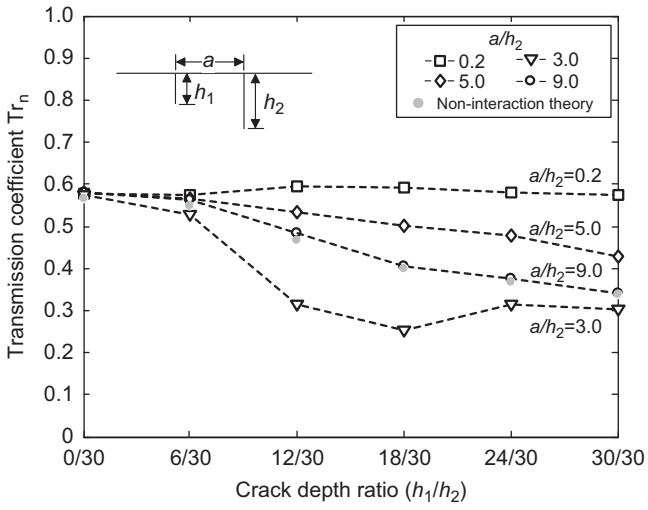

Fig. 11. Effects of crack spacing a/h on transmission coefficient for two cracks with different crack depths.

verified FE models. The depth of the second crack h_2 was fixed to 30 mm, while h_1 varies from 0 to 30 mm at an increment of 6 mm. In addition, four crack spacings of 6, 90, 150, and 270 mm were taken into account to investigate the combination effects of a/h_2 and h_1/h_2. The center frequency of incident surface waves in FE analyses was approximately 10 kHz, thus h_2/λ is around 0.24. Fig. 11 shows influence of the crack depth ratio h_1/h_2 on transmission coefficients in conjunction with the normalized crack spacing a/h_2. When h_1/h_2 is sufficiently small (e.g., 6/30), $\mathrm{Tr}_n(f_c)$ was dominated by the lager crack depth. In this case, interaction of surface waves between two cracks seems ignorable. However, increasing h_1/h_2 causes higher interaction between two cracks. In this case, effects of h_1/h_2 on $\mathrm{Tr}_n(f_c)$ should be understood along with the coupling effects of a/h_2. When a/h_2 is large enough (e.g., $a/h_2=9$), these two surface-breaking cracks can be regarded as two separated cracks so that the transmission coefficient of surface waves across these two cracks converges to $\mathrm{Tr}_1 \times \mathrm{Tr}_2$, where Tr_1 and Tr_2 are the transmission coefficients separately calculated from a single crack problem. In addition, when a/h_2 is very small (e.g. $a/h_2=0.2$), increasing h_1/h_2 does not have much impact on $\mathrm{Tr}_n(f_c)$.

5. Discussions and conclusions

For a single surface breaking crack, the measured surface wave transmission Tr across a crack depends on the normalized crack depth h/λ and sensor location x/λ. An analytical relation between Tr and h/λ is available for far-field measurement, i.e., when a/λ meets the far-field criterion. The near-field effect on surface wave transmission measurement has been studied by the authors for a single crack [28]. Results presented in this study indicate that the far-field criterion developed for a single crack case also applies to multi-crack models, when the sensor to crack spacing is large than the near-field size.

For distributed surface breaking cracks, the surface wave transmission is also affected by the crack spacing a/h. Cracks with very small spacing ($a/h\sim0.2$) can be regarded as a single crack, while cracks with very large spacing ($a/h\sim6$) will behave like individual separated cracks. For non-interacting cracks, the transmission across N cracks converges to $(\mathrm{Tr}_1)^N$. In the range of $a/h=2$–3, surface waves scattered from two adjacent cracks have strong interaction, and the surface wave transmission reaches the lowest value. This conclusion will be of interest to vibration insulation design to reach the lowest wave transmission by optimizing the depth and spacing of slots.

Because of complexity of the problem and many parameters involved, it is challenging to directly apply conclusions from this study to crack depth estimation. For each combination of crack number N and crack spacing a/h, a separate calibration curve is needed to uniquely determine the crack depth. However, when there is one major crack accompanied with many micro cracks, surface wave transmission is mainly governed by the major crack. Fig. 11 shows crack spacing has negligible influence on Tr when the depth ratio between the shallow and deep cracks is smaller than $6/30=0.2$. This finding is useful to determinate critical crack depth in materials with many micro-cracks, such as concrete.

References

[1] I.A. Viktorov, *Rayleigh Waves and Lamb Waves—Physical Theory and Application*, Plenum, New York, 1967.
[2] M. Hirao, H. Fukuoka, Y. Miura, Scattering of Rayleigh surface waves by edge cracks: numerical simulation and experiment, *The Journal of the Acoustical Society of America* 72 (1982) 602–606.
[3] J.D. Achenbach, L.M. Keer, D.A. Mendelsohn, Elastodynamic analysis of an edge crack, *Journal of Applied Mechanics* 47 (1980) 551–556.
[4] D.A. Mendelsohn, J.D. Achenbach, L.M. Keer, Scattering of elastic waves by a surface-breaking crack, *Wave Motion* 2 (1980) 277–292.
[5] Y.C. Angel, J.D. Achenbach, Reflection and transmission of obliquely incident Rayleigh waves by a surface-breaking crack, *The Journal of the Acoustical Society of America* 75 (1984) 313–319.
[6] C.H. Yew, K.G. Chen, D.L. Wang, An experimental study of interaction between surface waves and a surface breaking crack, *The Journal of the Acoustical Society of America* 75 (1984) 189–196.
[7] B. Masserey, E. Mazza, Analysis of the near-field ultrasonic scattering at a surface crack, *The Journal of the Acoustical Society of America* 118 (2005) 3585–3594.
[8] X. Jian, S. Dixon, N. Guo, R. Edwards, Rayleigh wave interaction with surface-breaking cracks, *Journal of Applied physics* 101 (2007) 064906.
[9] S.-H. Kee, J. Zhu, Using air-coupled sensors to evaluate the depth of a surface-breaking crack in concrete, *The Journal of the Acoustical Society of America* 127 (2010) 1279–1287.
[10] C. Zhang, J.D. Achenbach, Dispersion and attenuation of surface waves due to distributed surface-breaking, *The Journal of the Acoustical Society of America* 88 (1990) 1966–1992.
[11] C. Pecorari, Attenuation and dispersion of Rayleigh waves propagating on a cracked surface: an effective field approach, *Ultrasonics* 38 (2000) 754–760.
[12] C. Pecorari, Rayleigh wave dispersion due to a distribution of semi-ellitical surface-breaking cracks, *The Journal of the Acoustical Society of America* 103 (1998) 1383–1387.
[13] R.L. McNeill, B.E. Margason, F.M. Babcock, The role of soil dynamics in the design of stable test pads, *Proceedings, Guidance and Control Conference* (1965) 366–375.
[14] R.D. Woods, Screening of surface waves in soils, *ASCE Journal of Soil Mechenics* 94 (1968) 951–979.
[15] D.E. Beskos, B. Dasgupta, I.G. Vardoulakis, Vibration isolation using open or filled trenches, *Computational Mechanics* 1 (1986) 43–63.
[16] B. Dasgupta, D.E. Beskos, I.G. Vardoulakis, Vibration isolation using open or filled trenches part 2: 3-D homogeneous soil, *Computational Mechanics* 6 (1986) 129–142.
[17] S. Ahmad, T.M. Al-Hussaini, Simplified design for vibration screening by open and in-filled trenches, *Journal of Geotechnical Engineering* 117 (1991) 67–88.
[18] J. Zhu, J.S. Popovics, Non-contact imaging for surface-opening cracks in concrete with air-coupled sensors, *Materials and Structures* 38 (2005) 801–806.
[19] J. Oliver, F. Press, M. Ewing, Two-dimensional model seismology, *Geophysics* 19 (1953) 202–219.
[20] J.D. Achenbach, I.N. Komsky, Y.C. Lee, Y.C. Angel, Self-calibrating ultrasonic technique for crack depth measurement, *Journal of Nondestructive Evaluation* 11 (1992) 103–108.

[21] J.S. Popovics, W.-J. Song, M. Ghandehari, K.V. Subramaniam, J.D. Achenbach, S.P. Shah, Application of surface wave transmission measurements for crack depth determination in concrete, *ACI Materials Journal* 97 (2000) 127–135.
[22] W.-J. Song, J.S. Popovics, J.C. Aldrin, S.P. Shah, Measurement of surface wave transmission coefficient across surface-breaking cracks and notches in concrete, *The Journal of the Acoustical Society of America* 113 (2003) 717–725.
[23] D.N. Alleyne, P. Cawley, A two-dimensional Fourier transform method for the measurement of propagating multimode signals, *The Journal of the Acoustical Society of America* 89 (1991) 1159–1168.
[24] A. Zerwer, M.A. Polak, J.C. Santamarina, Wave propagation in thin Plexiglas plates; implications for Rayleigh waves, *NDT & E International* 33 (2000) 33–41.
[25] M. Liu, D.G. Gorman, Formulations of Rayleigh damping and its extensions, *Computers and Structures* 57 (1995) 277–285.
[26] J.H. Kim, H.-G. Kwak, Nondestructive evaluation of elastic properties of concrete using simulation of surface waves, *Computer-aided Civil and Infrastructure Engineering* 23 (2008) 611–624.
[27] S.-H. Kee, J. Zhu, Evaluation of distributed surface-breaking cracks in concrete using surface wave transmission method, *NDTCE' 09, Non-Destructive Testing in Civil Engineering*, Nantes, France, 2009.
[28] S.-H. Kee, J. Zhu, Effects of sensor locations on surface wave transmission measurements across a surface-breaking crack, *IEEE Transactions on Ultrasonics, Ferroelectrics and Frequency Control* 58 (2011) 427–436.